Available online at www.sciencedirect.com
SCIENCE DIRECT®
International Journal of Solids and Structures 42 (2005) 69–83
INTERNATIONAL JOURNAL OF SOLIDS and STRUCTURES
www.elsevier.com/locate/ijsolstr

Material characterization based on dual indenters

S. Swaddiwudhipong [a,*], K.K. Tho [a], Z.S. Liu [b], K. Zeng [c]

[a] *Department of Civil Engineering, National University of Singapore, Block E1A, 07-03, 1 Engineering Drive 2, Singapore 119260, Singapore*
[b] *Institute of High Performance Computing, 1 Science Park Road, #01-01, Singapore 117528, Singapore*
[c] *Institute of Material Research and Engineering, 3 Research Link, Singapore 117602, Singapore*

Received 3 March 2004; received in revised form 27 July 2004
Available online 18 September 2004

Abstract

Extensive large strain-large deformation finite element analyses were carried out to investigate the response of elasto-plastic materials obeying power law-strain hardening during the loading and unloading process of instrumented indentation with conical indenters of different apex angles. The relationships between the characteristics of the indentation load–displacement curves and the elasto-plastic material properties were computationally established. A reverse analysis algorithm based on load–displacement curves obtained from dual indenters was presented. It was demonstrated that the proposed reverse analysis algorithm can uniquely recover the elasto-plastic material properties from the load–displacement curves of two conical indenters with different apex angles. The numerical results obtained are in good agreement with published values.

Keywords: Dual indenters; Finite element analysis; Load–displacement indentation; Material characterization; Plastic deformation

1. Introduction

While the measurable quantity in an indentation test is usually the hardness of the materials, several methods have been proposed by researchers to extract the other basic mechanical properties, such as Young's modulus, yield strength and strain-hardening exponent from indentation load–displacement curves. Doerner and Nix (1986) and Oliver and Pharr (1992) proposed methods to obtain Young's modulus of materials from the unloading part of indentation load–displacement curves. Subsequently, Cheng and Cheng (1999b) derived a set of dimensionless functions to associate the characteristics of the indentation

* Corresponding author. Tel.: +65 68742173; fax: +65 67791635.
E-mail address: cvesomsa@nus.edu.sg (S. Swaddiwudhipong).

0020-7683/$ - see front matter © 2004 Elsevier Ltd. All rights reserved.
doi:10.1016/j.ijsolstr.2004.07.027

load–displacement curve with the elasto-plastic properties of the material. Based on three-dimensional finite-element simulations, Giannakopoulos and Suresh (1999) proposed a set of equations for reverse analysis of indentation experiments. Zeng and Chiu (2001) and Zeng and Shen (2002) proposed empirical methods to determine the Young's modulus and strain-hardening exponent from the unloading curve. Dao et al. (2001) proposed a new set of dimensionless functions and forward and reverse analysis scheme based on extensive finite element simulations. Bucaille et al. (2003) and Chollacoop et al. (2003) subsequently extended the method proposed by Dao et al. (2001) for forward and reverse analysis based on dual sharp indenters. More recently, Tho et al. (2004b) proposed a new method for interpretation of indentation load–displacement curves.

The uniqueness of the results from the reverse analysis process, which is an intrinsic characteristic of the problem, is a fundamental issue that needs to be addressed. If more than one sets of elasto-plastic material properties result in identical indentation load–displacement curves, any attempt to recover the elasto-plastic material properties from the indentation load–displacement curve will be futile. Various researchers who have studied the issue of uniqueness of the reverse analysis based on a single indenter arrived at somewhat different conclusions (Cheng and Cheng, 1999a; Zeng and Chiu, 2001; Dao et al., 2001; Chollacoop et al., 2003; Capehart and Cheng, 2003). Tho et al. (2004b) confirmed the non-uniqueness of results obtained from the reverse analysis of a single indenter by demonstrating that the relationship between the elasto-plastic material properties and the resulting load–displacement curve is not one-to-one.

In the present study, finite element analyses are carried out to investigate the response of elasto-plastic materials obeying power law strain-hardening during instrumented indentation using two different indenters. The surfaces describing the variation of C/Y and W_R/W_T with E^*/Y and n are computationally derived for each indenter. It is demonstrated that unique recovery of the elasto-plastic material properties is only possible if the load–displacement curves of at least two different indenters are used in the analysis.

2. Finite element simulation of indentation test

Large strain-large deformation axisymmetric finite element analyses were carried out using ABAQUS, a commercial general purpose finite element package. Conical indenters with half-angles of 60.0° and 70.3° are modelled as rigid bodies in the finite element models. The finite element mesh for the target material covering a $200 \times 200\,\mu m^2$ area consists of 28,900 four-node, bilinear axisymmetric quadrilateral elements. A finer mesh is used near the contact region where high stress concentration is expected and the element size is gradually increased further away from this region. Fig. 1 illustrates the finite element mesh in the vicinity of the contact region. At the maximum indentation depth of 5 μm, there are at least 50 elements at the contact interface. As illustrated in Fig. 2, the size of the domain adopted in the analysis is sufficiently large to simulate semi-infinite boundary conditions and is insensitive to the far-field effect. The convergence of the mesh used in the analyses was verified through convergence studies as depicted in Fig. 3. As the effect of friction is negligible for indenters with half-angle larger than 60° (Bucaille et al., 2003), frictionless contact is assumed in the present finite element model.

Materials obeying power law strain-hardening were considered in this study. For such materials, the uniaxial true stress–true strain relationship can be expressed as

$$\sigma = E\varepsilon \quad \text{for } \sigma \leqslant Y, \tag{1a}$$

$$\sigma = R\varepsilon^n \quad \text{for } \sigma \geqslant Y. \tag{1b}$$

In Eq. (1), E is the Young's modulus, Y is the yield stress, R is the strength coefficient and n is the strain-hardening exponent.

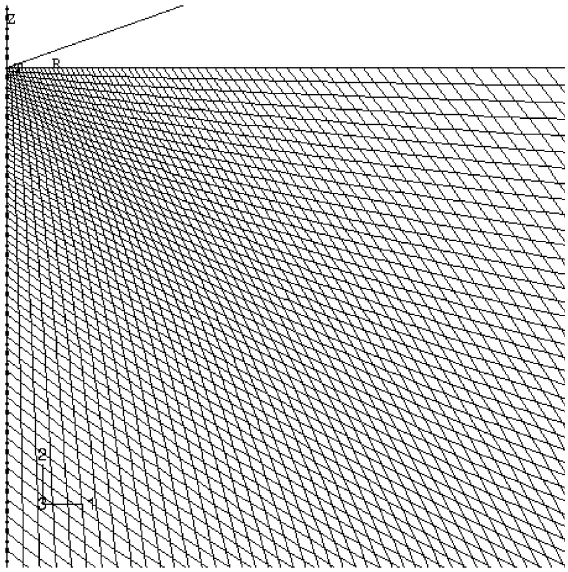

Fig. 1. Finite element mesh in the vicinity of contact region.

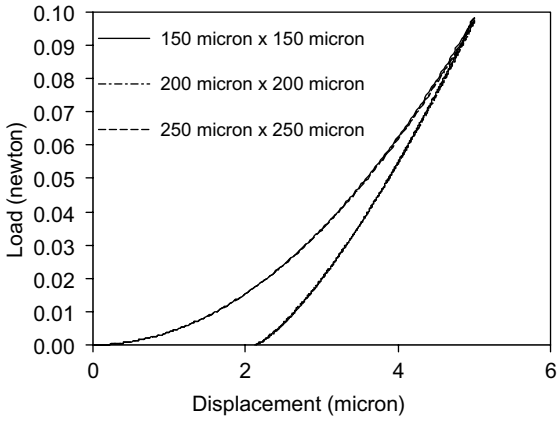

Fig. 2. Indentation diagrams for various domain sizes.

By enforcing continuity at $\sigma = Y$,

$$R = Y\left(\frac{E}{Y}\right)^{n}. \tag{2}$$

The elasticity effect of the indenter can be considered in the analysis through the replacement of the actual Young's modulus, E of the targeted materials by a reduced Young's modulus, expressed in Eq. (3) (Giannakopoulos and Suresh, 1999; Dao et al., 2001; Chollacoop et al., 2003).

$$E^{*} = \left[\frac{1-\nu^{2}}{E} + \frac{1-\nu_{i}^{2}}{E_{i}}\right]^{-1}. \tag{3}$$

In Eq. (3), E^{*} is the reduced Young's modulus, E_i and ν_i are the Young's modulus and Poisson's ratio of the indenter.

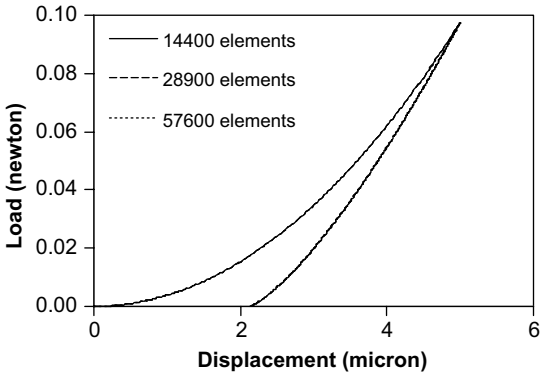

Fig. 3. *h*-Convergence study on indentation curves.

3. Fundamental aspects of load–displacement curves

A typical load–displacement curve in an indentation experiment is shown in Fig. 4. It is generally believed that the curvature of the loading curve (C), the gradient at initial part of the unloading curve (S) and the ratio of the indentation work done to total work done (W_R/W_T) are three independent quantities which can be obtained from a single load–displacement curve (Giannakopoulos and Suresh, 1999; Dao et al., 2001). For a constant value of Poisson's ratio and indenter geometry, it has been shown that these three quantities are functions of the three elasto-plastic material properties (E^*, Y, n) (Tho et al., 2004b; Cheng and Cheng, 1998b). The notion of independence of the three quantities obtained from a single load–displacement curve has significant implications on the uniqueness of the reverse analysis process. The independence of the three quantities and the fact that they are functions of only E^*, Y, n for a particular indenter geometry and a constant value of Poisson's ratio suggests that the reverse analysis process involving the indentation load–displacement curve of a single indenter should yield unique solution due to the existence of three independent relationships to solve for three unknowns. However, Tho et al. (2004b), Cheng and Cheng (1999a) and Capehart and Cheng (2003) have shown that the reverse analysis process based on a single indenter is non-unique, implying some form of dependency between the three quantities. It is apparent from Tho et al. (2004a) that knowing the values of two of the three quantities leads to the value of the third quantity. Hence, from the load–displacement curve of a single indenter, there exist only two independent relationships to solve for the three unknowns.

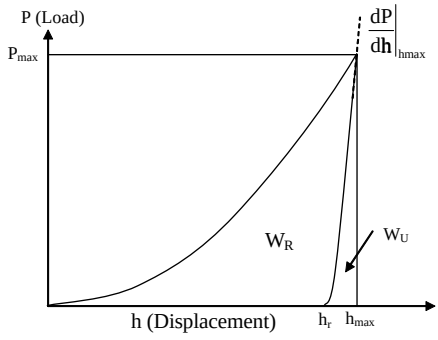

Fig. 4. Schematic representation of load–displacement curve.

The non-uniqueness of the results obtained from reverse analysis of a single indenter could be overcome by combining the information drawn from the indentation load–displacement curves of two different indenters. In the present study, the work of Tho et al. (2004b) is extended to approach involving dual indenters. In their work, the relationship between W_R/W_T and the three elasto-plastic material properties (E^*, Y, n) is found to be essential in the solution process. Hence, only one of the two remaining quantities (C, S) needs to be considered in the analysis. Since the curvature of the loading curve, C can be accurately and unambiguously evaluated from the experimental indentation load–displacement curve, C is considered instead of S in the present study.

3.1. Loading curve

The loading part of an instrumented sharp indentation generally follows Kick's law which can be expressed as

$$P = Ch^2, \tag{4}$$

where P is the indentation load, h is the penetration depth measured from the surface and C is a constant curvature.

The projected contact area for indenters with linear relationships between penetration depth and contact radius (conical, Berkovich and Vickers) can be expressed as

$$A = kh^2, \tag{5}$$

where k is a constant for a particular material and an indenter geometry.

Dividing Eq. (4) by Eq. (5) leads to

$$p_{ave} = \frac{P}{A} = \frac{C}{k} = \text{constant}. \tag{6}$$

Based on the relationships derived by Luk et al. (1991),

$$\frac{p_{ave}}{Y} = f\left(\frac{E^*}{Y}, n\right). \tag{7}$$

By combining Eqs. (6) and (7), the following relationship between C and the three material parameters (E^*, Y, n) can be established:

$$\frac{C}{Y} = f_{1,\theta}\left(\frac{E^*}{Y}, n\right), \tag{8}$$

where θ is the half-angle of the indenter.

3.2. Relationship between indentation work and total work done

Cheng and Cheng (1998a) derived the following dimensionless function:

$$\frac{W_T - W_u}{W_T} = \prod_{\omega}\left(\frac{Y}{E}, v, \theta\right), \tag{9}$$

where W_T is the area under the loading curve, W_u is the area under the unloading curve, v is the Poisson's ratio and θ is the half angle of the indenter.

Denoting $(W_T - W_u)$ by W_R, Eq. (10) is expressed in the following form for a particular value of Poisson's ratio and half-angle of the indenter:

$$\frac{W_R}{W_T} = f_{2,\theta}\left(\frac{E^*}{Y}, n\right). \tag{10}$$

3.3. Surfaces describing functions $f_{1,60.0}$, $f_{1,70.3}$, $f_{2,60.0}$ and $f_{2,70.3}$

The validity of Eqs. (8) and (10) were verified by Tho et al. (2004b). Variations of C/Y and W_R/W_T with respect to E^*/Y and n for each indenter are best illustrated by the surfaces described by functions $f_{1,60.0}(E^*/Y,n)$, $f_{1,70.3}(E^*/Y,n)$, $f_{2,60.0}(E^*/Y,n)$ and $f_{2,70.3}(E^*/Y,n)$. The data for construction of these surfaces were obtained numerically through more than 1000 large strain, large deformation finite element analyses encompassing a domain of E^*/Y from 10 to 1000 and n varying from 0.0 to 0.6. A constant Poisson's ratio of 0.33 is used throughout this study.

The functions $f_{1,60.0}(E^*/Y,n)$, $f_{1,70.3}(E^*/Y,n)$, $f_{2,60.0}(E^*/Y,n)$ and $f_{2,70.3}(E^*/Y,n)$ are computationally determined and the four functions fit all data points within a $\pm 1.5\%$ error. The surfaces describing functions $f_{1,60.0}(E^*/Y,n)$, $f_{1,70.3}(E^*/Y,n)$, $f_{2,60.0}(E^*/Y,n)$and $f_{2,70.3}(E^*/Y,n)$ are depicted in Figs. 5–8, respectively with each small circle representing a numerical data point.

3.4. Relationship between W_R/W_T and h_r/h_{max}

Based on the results of more than 1000 finite element analyses, the relationship between the quantities h_r/h_{max} and W_R/W_T are displayed in Fig. 9. The relationships proposed by Cheng and Cheng (2002) and Tho et al. (2004b) are also included in the same figure for comparison purpose. Fig. 9 demonstrates the strong correlation between the two quantities and linear relationship is observed for $W_R/W_T > 0.5$, which corresponds to $E^*/Y \geqslant 60$ and $0.0 \leqslant n \leqslant 0.6$. Most engineering metals and alloys fall within this range of material properties.

Since a one-to-one relationship exists between h_r/h_{max} and W_R/W_T, the determination of either quantity would lead to the other. However, as W_R/W_T is determined based on all the data points on the load–displacement curve while h_r/h_{max} is determined from a single point on the load–displacement curve, it is expected that the error in adopting W_R/W_T as the basic parameter will be significantly less than that of h_r/h_{max}.

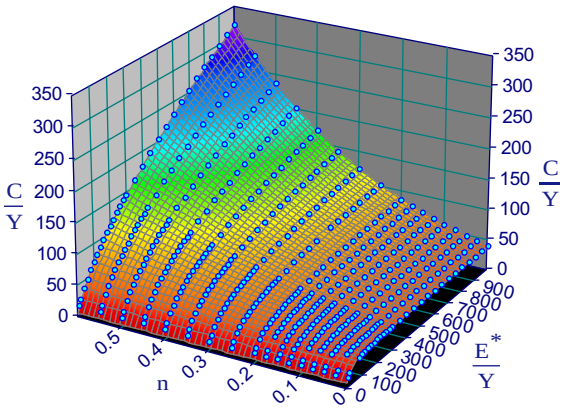

Fig. 5. Surface described by $f_{1,60.0}(E^*/Y,n)$.

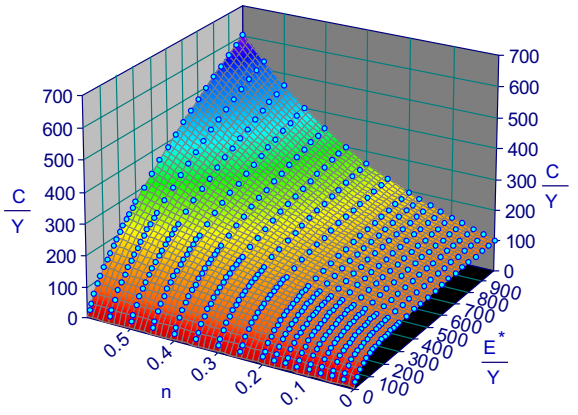

Fig. 6. Surface described by $f_{1,70.3}(E^*/Y, n)$.

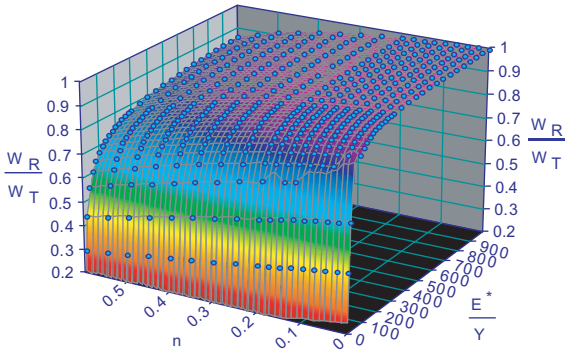

Fig. 7. Surface described by $f_{2,60.0}(E^*/Y, n)$.

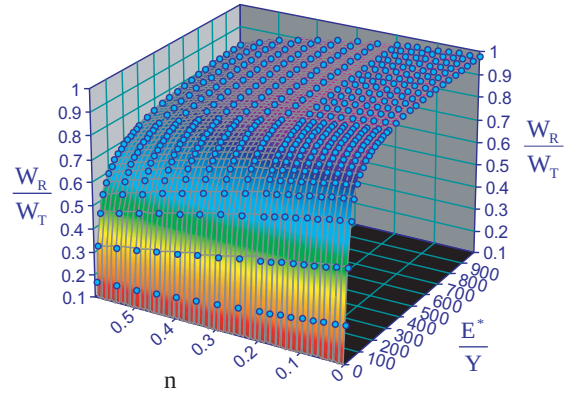

Fig. 8. Surface described by $f_{2,70.3}(E^*/Y, n)$.

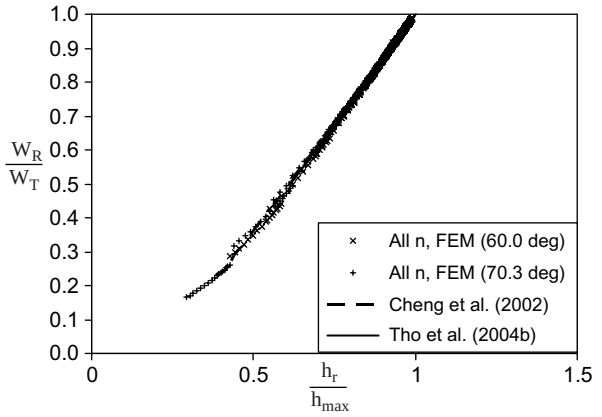

Fig. 9. Relationships between $\frac{W_R}{W_T}$ and $\frac{h_r}{h_{max}}$.

4. Forward and reverse analysis algorithms

4.1. Forward analysis scheme

The forward analysis scheme enables the prediction of the load–displacement response for a material when the elasto-plastic properties (E^*, Y, n) are provided as inputs. With the availability of the surfaces describing functions $f_{1,60.0}(E^*/Y, n)$, $f_{1,70.3}(E^*/Y, n)$, $f_{2,60.0}(E^*/Y, n)$ and $f_{2,70.3}(E^*/Y, n)$, the forward analysis scheme is straightforward. By substituting the elasto-plastic properties (E^*, Y, n) into Eqs. (8) and (10), the curvature of the loading curve (C) and the ratio of indentation work done to total work done (W_R/W_T) can be determined for each indenter.

4.2. Reverse analysis scheme

The reverse analysis scheme enables the determination of the elasto-plastic properties (E^*, Y, n) from indentation load–displacement curves. By substituting $\theta = 60.0°$ and $70.3°$ into Eqs. (8) and (10), Eqs. (11)–(14) can be obtained:

$$\left.\frac{C}{Y}\right|_{60.0°} = f_{1,60.0°}\left(\frac{E^*}{Y}, n\right), \tag{11}$$

$$\left.\frac{C}{Y}\right|_{70.3°} = f_{1,70.3°}\left(\frac{E^*}{Y}, n\right), \tag{12}$$

$$\left.\frac{W_R}{W_T}\right|_{60.0°} = f_{2,60.0°}\left(\frac{E^*}{Y}, n\right), \tag{13}$$

$$\left.\frac{W_R}{W_T}\right|_{70.3°} = f_{2,70.3°}\left(\frac{E^*}{Y}, n\right). \tag{14}$$

Dividing Eq. (11) by Eq. (12) leads to

$$\frac{C_{60.0°}}{C_{70.3°}} = \frac{f_{1,60.0°}\left(\frac{E^*}{Y}, n\right)}{f_{1,70.3°}\left(\frac{E^*}{Y}, n\right)}. \tag{15}$$

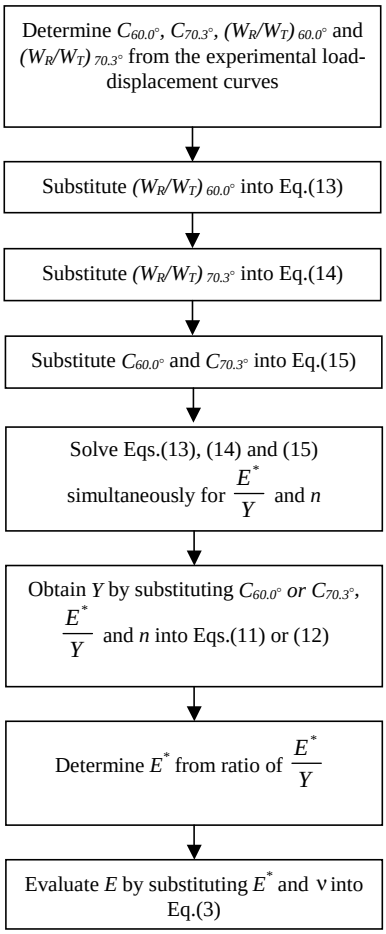

Fig. 10. Flowchart illustrating reverse analysis algorithm.

From the indentation load–displacement curves of both indenters, the quantities $C_{60.0^\circ}$, $C_{70.3^\circ}$, $(W_R/W_T)_{60.0^\circ}$ and $(W_R/W_T)_{70.3^\circ}$ can be determined. The problem can be solved by first searching for a combination of E^*/Y and n that satisfy Eqs. (13)–(15) simultaneously. Once a set of E^*/Y and n is found, Y can be evaluated by substituting C, E^*/Y and n into Eq. (11) or (12). Consequently, E^* can be evaluated from the ratio of E^*/Y established earlier. The actual Young's modulus E can then be obtained from Eq. (3). The reverse analysis algorithm is summarized in the flowchart shown in Fig. 10. The implementation of the forward and reverse analysis algorithms and the uniqueness of reverse analysis will be demonstrated in the next section.

5. Uniqueness of results from reverse analysis

Kalpakjian and Schmid (2003) and MatWeb (2003) provide the values of E^*, Y and n of Al6061-T651 as 72.36 GPa, 275 MPa and 0.05, respectively. These values are consistent with those presented by Luk et al. (1991). Finite element analyses were carried out using these material properties as input parameters and the resulting load–displacement curves are depicted in Fig. 11.

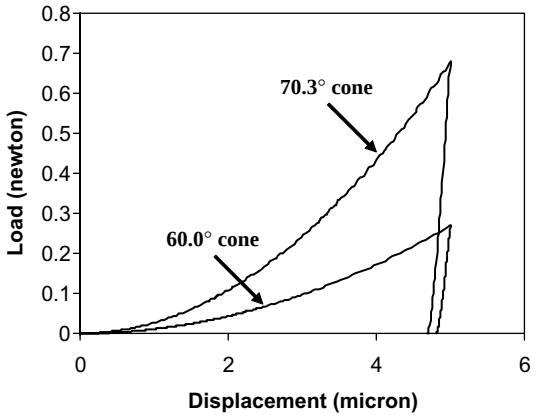

Fig. 11. Numerical load–displacement curves for Al6061-T651.

The finite element results and the forward analysis predictions for Al6061-T651 are tabulated (Table 1). The experimental results of Dao et al. (2001) and Chollacoop et al. (2003) are also included for comparison. It can be observed that the forward analysis algorithm can accurately predict the quantities $C_{60.0^\circ}$, $C_{70.3^\circ}$, $(W_R/W_T)_{60.0^\circ}$ and $(W_R/W_T)_{70.3^\circ}$ of the numerical indentation load–displacement curves shown in Fig. 11 despite the fact that finite element results of Al6061-T651 were not used in the computation of surfaces describing functions $f_{1,60.0}(E^*/Y,n)$, $f_{1,70.3}(E^*/Y,n)$, $f_{2,60.0}(E^*/Y,n)$ and $f_{2,70.3}$ $(E^*/Y,n)$. The forward analysis algorithm is also able to predict the experimental results of Dao et al. (2001) and Chollacoop et al. (2003) within a $\pm 5\%$ accuracy.

Reverse analysis is then carried out using the finite element results shown in Table 1 as inputs. Substituting the values of $C_{60.0^\circ}$, $C_{70.3^\circ}$, $(W_R/W_T)_{60.0^\circ}$ and $(W_R/W_T)_{70.3^\circ}$ into Eqs. (13)–(15) provides,

$$f_{2,60.0^\circ}\left(\frac{E^*}{Y},n\right)=0.9521, \tag{16}$$

$$f_{2,70.3^\circ}\left(\frac{E^*}{Y},n\right)=0.9214, \tag{17}$$

$$\frac{f_{1,60.0^\circ}\left(\frac{E^*}{Y},n\right)}{f_{1,70.3^\circ}\left(\frac{E^*}{Y},n\right)}=0.3949. \tag{18}$$

Table 1
Forward analysis on Al6061-T651

	$C_{60.0^\circ}$ (N m^{-2})	$C_{70.3^\circ}$ (N m^{-2})	$(W_R/W_T)_{60.0^\circ}$	$(W_R/W_T)_{70.3^\circ}$
Finite element analysis	1.074E+10	2.720E+10	0.9521	0.9214
Forward analysis predictions	1.071E+10	2.713E+10	0.9521	0.9220
Dao et al. (2001) (average of 6 sets of results for Berkovich indenter)	–	2.740E+10	–	0.8960
Chollacoop et al. (2003) (average of 3 sets of results for 60.0° cone indenter)	1.127E+10	–	–	–

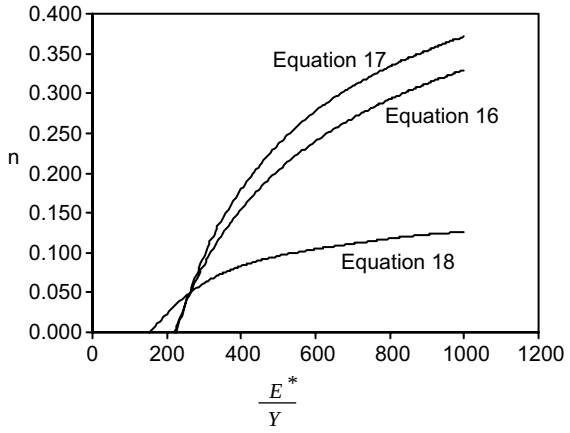

Fig. 12. Graphical representations of Eqs. (16)–(18).

The solution to the reverse analysis problem can be obtained by solving Eqs. (16)–(18) simultaneously for the values of E^*/Y and n. Graphically, the solution is represented by the point of intersection of these equations. As functions $f_{1,60.0}(E^*/Y,n)$, $f_{1,70.3}(E^*/Y,n)$, $f_{2,60.0}(E^*/Y,n)$ and $f_{2,70.3}(E^*/Y,n)$ have been established earlier, the graphical representations of Eqs. (16)–(18) are shown in Fig. 12. It can be observed from Fig. 12 that Eqs. (16)–(18) intersect each other at practically a point across the domain, implying that there is only one admissible solution. Hence, contrary to the non-uniqueness of the reverse analysis algorithm based on a single indenter, the procedure involving results from dual indenters produces a unique set of solutions. Physically, the uniqueness of the solution based on dual indenters can be explained by the fact that combinations of material properties that result in identical load–displacement curve for one indenter will provide different load–displacement curves for dual indenters. Tho et al. (2004b) have identified at least six other combinations of material properties that give the same load–displacement response as Al6061-T651 for a conical indenter with a half-angle of 70.3°. Forward analyses for both indenters are carried out using the seven sets of material properties as inputs and the calculated loading curvature are shown in Table 2. It is apparent that all the seven combinations of material properties result in virtually the same value of loading curvature for the indenter with a half-angle of 70.3°. However, the values of loading curvature for the indenter with a half-angle of 60.0 vary significantly.

Table 2
Forward analyses results for different combination of material properties

Material properties			C (GPa)	
E^* (GPa)	Y (MPa)	n	60.0° half-angle cone	70.3° half-angle cone
71.1	296.2	0.020	10.55	27.15
72.4	275.0	0.050	10.71	27.13
76.7	213.0	0.144	11.36	27.14
80.2	160.3	0.230	11.89	27.13
83.4	119.1	0.302	12.27	27.09
84.8	98.7	0.342	12.50	27.14
86.1	86.1	0.367	12.63	27.11
Maximum percentage difference			19.72	0.22
Minimum percentage difference			1.04	0.00

Table 3
Summary of finite element results for Al7075, steel, iron and zinc

Material	Conical indenter with half-angle of 60.0°		Conical indenter with half-angle of 70.3°	
	$C_{60.0^\circ}$ (GPa)	$C_{70.3^\circ}$ (GPa)	$(W_R/W_T)_{60.0^\circ}$	$(W_R/W_T)_{70.3^\circ}$
Al7075	20.362	46.555	0.903	0.853
Steel	23.907	59.272	0.960	0.937
Iron	24.598	55.513	0.949	0.925
Zinc	6.556	13.574	0.729	0.621

Table 4
Summary of reverse analysis results

	Al6061	Al7075	Steel	Iron	Zinc
E^* (GPa)					
Original	72.4	73.4	194.3	170.8	10.0
Predicted	72.0	73.3	196.3	171.0	9.6
Deviation (%)	−0.5	−0.2	1.1	0.2	−3.8
E (GPa)					
Original	69.0	70.1	210.0	180.0	9.0
Predicted	68.6	69.9	212.7	180.3	8.7
Deviation (%)	−0.6	−0.2	1.3	0.2	−3.8
Y (MPa)					
Original	275.0	500.0	500.0	300.0	300.0
Predicted	276.9	505.8	488.2	293.7	306.8
Deviation (%)	0.7	1.2	−2.4	−2.1	2.3
n					
Original	0.050	0.122	0.100	0.250	0.050
Predicted	0.049	0.118	0.107	0.255	0.000
Deviation	0.001	0.004	−0.007	−0.005	0.050

Additional finite element analyses were carried out to simulate indentation experiments on Al7075, steel, iron and zinc. The typical elasto-plastic material properties (Bucaille et al., 2003) of these materials are used as inputs to the finite element model. The ratio of E^*/Y for these materials vary from 33 to 570 while the values of n range from 0.05 to 0.25. The finite element results are summarised in Table 3.

The solution procedure described in Section 4.2 is then applied using the finite element results depicted in Tables 1 and 3 as inputs. The material properties predicted by the proposed reverse analysis algorithm are shown in Table 4 together with the original material properties. It can be observed that the proposed reverse analysis algorithm predicts the elasto-plastic material properties reasonably accurately.

6. Sensitivity analysis

The sensitivity of the predicted elasto-plastic material properties to perturbations in the four input parameters ($C_{60.0^\circ}$, $C_{70.3^\circ}$, $(W_R/W_T)_{60.0^\circ}$ and $(W_R/W_T)_{70.3^\circ}$) was investigated. Chollacoop et al. (2003) noted that typical experimental scatter for curvature of the loading curve, C is $\pm 2\%$ while that for the ratio of indentation work-done to total work-done, W_R/W_T is $\pm 1\%$. The perturbations in the four input parameters are assumed to occur simultaneously and Monte Carlo simulations were carried out to investigate the sensitivity of the reverse analysis. The results of the Monte Carlo simulations are depicted in Figs. 13–15. As

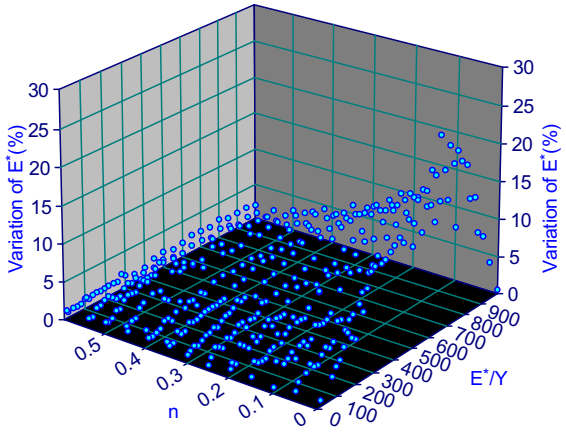

Fig. 13. Sensitivity study on the values of E^*.

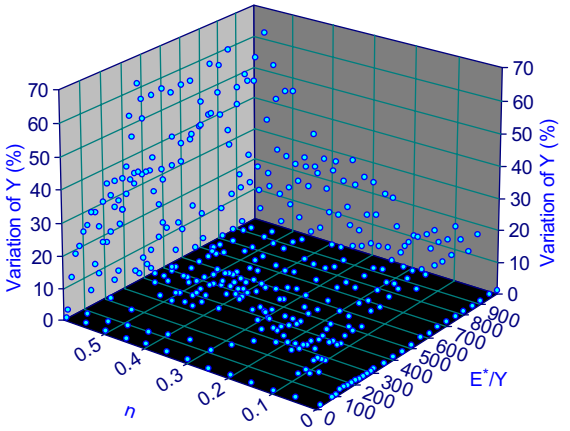

Fig. 14. Sensitivity study on the values of Y.

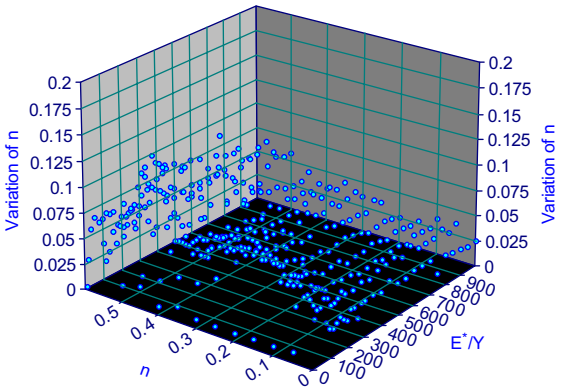

Fig. 15. Sensitivity study on the values of n.

depicted in Fig. 13, the maximum variation of E^* due to perturbations of $C_{60.0^\circ}$, $C_{70.3^\circ}$, $(W_R/W_T)_{60.0^\circ}$ and $(W_R/W_T)_{70.3^\circ}$ is close to 20% when $n = 0.0$. The variation of E^* in other regions in the domain is less than 5%.

It can be observed from Fig. 14 that Y exhibits rather strong sensitivity to perturbations in input parameters, especially for regions with large n values. The maximum variation of Y is approximately 70%. At regions with n values less than 0.4, the variation of Y due to perturbations in input parameters is capped at 30%. Fig. 15 illustrates the variation of n in the Monte Carlo simulations. The maximum variation of n in the domain is about 0.1 for the large value of n of 0.6. At most other regions in the domain, the variation of n is less than 0.05.

Qualitative estimates of the sensitivity of the results from the reverse analysis with respect to variations of $(W_R/W_T)_{60.0^\circ}$ and $(W_R/W_T)_{70.3^\circ}$ can be obtained from careful inspection of Figs. 7 and 8. The regions with steeper gradients will exhibit weaker sensitivity to variations of $(W_R/W_T)_{60.0^\circ}$ and $(W_R/W_T)_{70.3^\circ}$. Therefore, the sensitivity of the predicted material properties due to variations of the input parameters is essentially an intrinsic characteristic of the problem. A plausible approach to reduce the sensitivity of the predicted material properties to perturbations in input parameters would be to introduce a higher degree of redundancy by incorporating the results of more indenters. The reverse analysis algorithm illustrated in Section 4.2 can be easily extended for this purpose.

7. Conclusion

E^*/Y and n are found to be the two key parameters that govern the characteristics of load–displacement curves for elasto-plastic materials. The numerical results obtained in the present study are in good agreement with published experimental values. Information derived from the load–displacement curves of two indenters with different geometries is essential for unique recovery of the three elasto-plastic material properties. The proposed reverse analysis algorithm enabled the Young's modulus to be determined without the need to evaluate the slope at the initial part of the unloading curve. The sensitivity studies indicate that the predicted material properties deviate somewhat from the actual material properties in most regions but differ substantially in certain ranges at the extreme values of n. The proposed reverse analysis algorithm can be easily extended for multi-indenters. Improved accuracy can be expected when more than two indenters are adopted.

References

Bucaille, J.L., Stauss, S., Felder, E., Michler, J., 2003. Determination of plastic properties of metals by instrumented indentation using different sharp indenters. Acta Materialia 51, 1663–1678.

Capehart, T.W., Cheng, Y.T., 2003. Determining constitutive models from conical indentation: sensitivity analysis. Journal of Material Research 18 (4), 827–832.

Cheng, Y.T., Cheng, C.M., 1998a. Relationships between hardness, elastic modulus, and the work of indentation. Applied Physics Letters 73 (5), 614–616.

Cheng, Y.T., Cheng, C.M., 1998b. Scaling approach to conical indentation in elastic–plastic solids with work hardening. Journal of Applied Physics 84 (3), 1284–1291.

Cheng, Y.T., Cheng, C.M., 1999a. Can stress–strain relationships be obtained from indentation curves using conical and pyramidal indenters? Journal of Material Research 14 (9), 3493–3496.

Cheng, Y.T., Cheng, C.M., 1999b. Scaling relationships in conical indentation of elastic-perfectly plastic solids. International Journal of Solids and Structures 36, 1231–1243.

Cheng, Y.T., Li, Z., Cheng, C.M., 2002. Scaling relationships for indentation measurements. Philosophical Magazine A 82 (10), 1821–1829.

Chollacoop, N., Dao, M., Suresh, S., 2003. Depth-sensing instrumented indentation with dual sharp indenters. Acta Materialia 51, 3713–3729.

Dao, M., Chollacoop, N., Van Vliet, K.J., Venkatesh, T.A., Suresh, S., 2001. Computational modelling of the forward and reverse problems in instrumented sharp indentation. Acta Materialia 49, 3899–3918.

Doerner, M.F., Nix, W.D., 1986. A method for interpreting the data from depth-sensing indentation instruments. Journal of Material Research 1 (4), 601–609.

Giannakopoulos, A.E., Suresh, S., 1999. Determination of elastoplastic properties by instrumented sharp indentation. Scripta Materialia 40 (10), 1191–1198.

Kalpakjian, S., Schmid, S.R., 2003. Manufacturing Processes for Engineering Materials. Prentice-Hall, New Jersey.

Luk, V.K., Forrestal, M.J., Amos, D.E., 1991. Dynamic spherical cavity expansion of strain-hardening materials. Journal of Applied Mechanics 58, 1–6.

MatWeb, 2003. Automation Creations, Inc. Available from: <http://www.matweb.com>.

Oliver, W.C., Pharr, G.M., 1992. An improved technique for determining hardness and elastic modulus using load and displacement sensing indentation experiments. Journal of Material Research 7 (6), 1564–1583.

Tho, K.K., Swaddiwudhipong, S., Liu, Z.S., Zeng, K., Hua, J., 2004a. Uniqueness of reverse analysis from conical indentation tests. Journal of Material Research 19 (8), 2498–2502.

Tho, K.K., Swaddiwudhipong, S., Liu, Z.S., Zeng, K., 2004b. Simulation of instrumented indentation and material characterization. Material Science and Engineering A, in press.

Zeng, K., Chiu, C.H., 2001. An analysis of load–penetration curves from instrumented indentation. Acta Materialia 49, 3539–3551.

Zeng, K., Shen, L., 2002. A new analysis of nanoindentation load–displacement curves. Philosophical Magazine A 82 (10), 2223–2229.